iScience

CellPress
OPEN ACCESS

Article

Impaired interferon-γ signaling promotes the development of silicosis

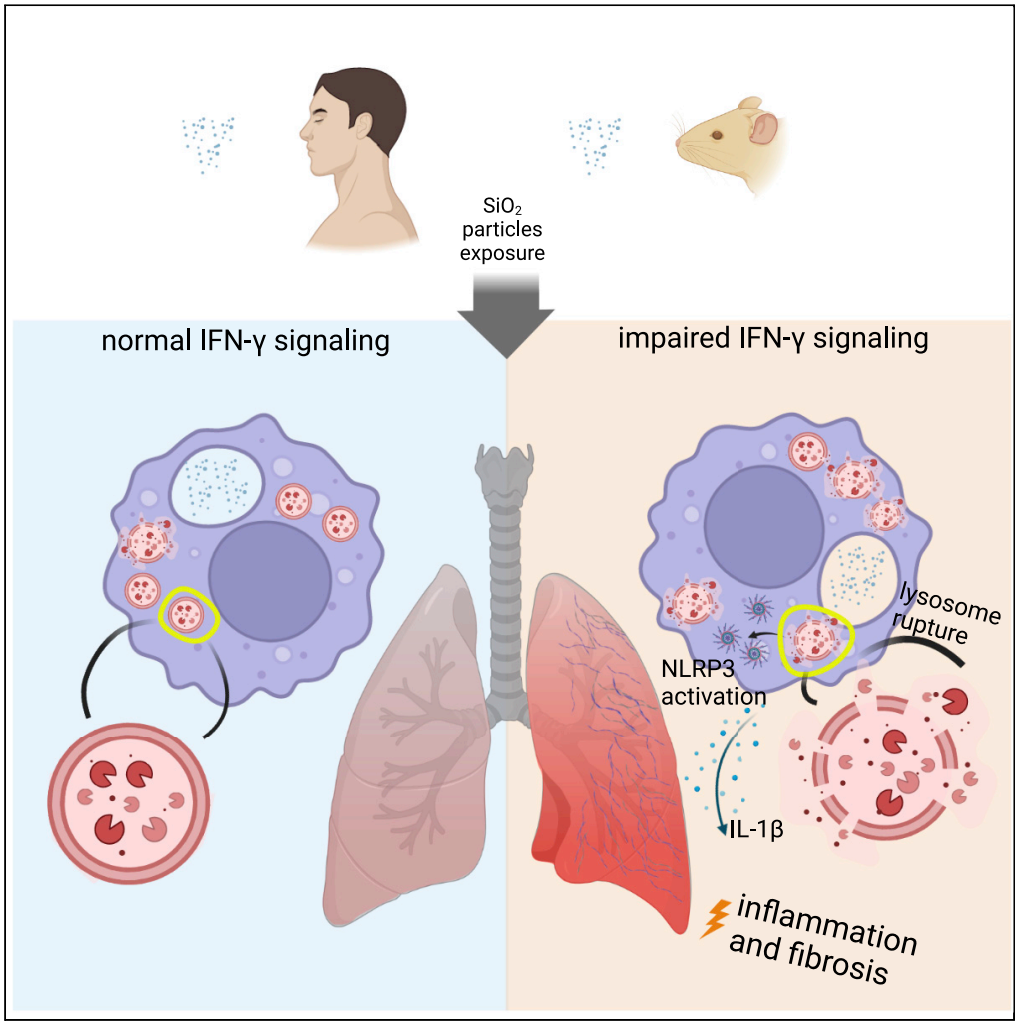

Zhouyangfan Peng, Mingwu Duan, Yiting Tang, ..., Timothy R. Billiar, Ben Lu, Fang Liang

xybenlu@csu.edu.cn (B.L.)
liangfang924@163.com (F.L.)

Highlights

IFN-γ signaling lacking in bronchoalveolar lavage myeloid cells from silicosis patients

Loss of IFN-γ signaling promotes silicosis via NLRP3 inflammasome

Loss of IFN-γ signaling triggers lysosomal damage to activate NLRP3 inflammasome

Peng et al., iScience 25, 104647
July 15, 2022 © 2022
https://doi.org/10.1016/j.isci.2022.104647

iScience

CellPress
OPEN ACCESS

Article

Impaired interferon-γ signaling promotes the development of silicosis

Zhouyangfan Peng,[1,12] Mingwu Duan,[1,12] Yiting Tang,[2] Jianfeng Wu,[3] Kai Zhao,[1] Yanjun Zhong,[6] Zhihui He,[1] Jie Meng,[4,5] Fangping Chen,[1] Xianzhong Xiao,[7,8] Haichao Wang,[9] Timothy R. Billiar,[10] Ben Lu,[1,7,8,*] and Fang Liang[1,11,*]

SUMMARY

Silicosis is caused by inhalation of crystalline silica dust particles and known as one of the most serious occupational diseases worldwide. However, little is known about intrinsic factors leading to disease susceptibility. Single-cell sequencing of bronchoalveolar lavage fluid cells of mine workers with silicosis and their co-workers who did not develop silicosis revealed that the impaired interferon (IFN)-γ signaling in myeloid cells was strongly associated with the occurrence of silicosis. Global or myeloid cell-specific deletion of interferon γ receptor (IFN-γR) markedly enhanced the crystalline silica-induced pulmonary injury in wild-type but not in NLRP3 deficient mice. *In vitro*, IFN-γ priming of macrophages suppressed the crystalline silica-induced NLRP3 inflammasome activation partly by inducing the formation of spacious phagosomes with relatively reduced ratio of crystalline silica/phagosomal areas volumes to resistant crystalline silica-induced lysosomal membrane damage. Thus, these findings provide molecular insights into the intricate mechanisms underlying innate immunity-mediated host responses to environmental irritants.

INTRODUCTION

Silicosis is a chronic interstitial pulmonary disease caused by the inhalation of free crystalline silica dust (The LRM, 2019). It is characterized by granulomatous lung inflammation, delayed pulmonary interstitial fibrosis and progressive respiratory dysfunction (Cao et al., 2020; Cullinan et al., 2017). Although preventive efforts have been made, silicosis is still one of the most important occupational diseases worldwide (Cullinan et al., 2017). China with more than 500,000 cases recorded has more than 6000 new cases of silicosis each year and more than 24,000 deaths annually (Leung et al., 2012). As a major problem for workers in small-scale mines, silicosis is irreversible and not therapeutically curable. However, only a small proportion of workers with prolonged inhalation of free crystalline silica eventually develop silicosis (Casey and Mazurek,2019; Wang et al., 2020). It was previously believed that the susceptibility of silicosis might be because of individual genetic variation (Ohtsuka et al., 2006). Some studies report that the polymorphisms in genes encoding proinflammatory cytokines or growth factors are associated with the occurrence of silicosis (Salum et al., 2020a; Wang et al., 2012). However, the functional relevance of the gene polymorphisms to the development of silicosis has not been validated (Salum et al., 2020b; Wu et al., 2008). Thus, the underlying mechanisms of mammalian susceptibility to silicosis remain largely unknown.

Accumulating evidence shows that deregulated pulmonary immune responses drive the development and progression of silicosis (Lee et al., 2017; Pollard,2016). Alveolar macrophages orchestrate lung inflammation in responses to both infectious and non-infectious agents. Phagocytosis of the inhaled crystalline silica by alveolar macrophages results in lysosomal damage, which elicits the activation of NOD-like receptor family pyrin domain-containing 3 (NLRP3) inflammasome, an intracellular protein complex that mediates the activation of caspase-1 and the subsequent maturation of proinflammatory cytokines including interleukin (IL)-1β and IL-18(Cassel et al., 2008; Dostert et al., 2008; Hornung et al., 2008). In murine silicosis models, deletion of the genes encoding NLRP3 inflammasome components markedly attenuates silica crystals-induced granulomatous lung inflammation and pulmonary fibrosis (Cassel et al., 2008; Dostert et al., 2008). Similarly, other immune cells such as dendritic cells, lymphocytes and mast cells also occupy important roles in silica crystals-induced pulmonary interstitial fibrosis(Benmerzoug et al., 2018; Liu et al.,

[1]Department of Hematology and Critical Care Medicine, The Third Xiangya Hospital, Central South University, Changsha 410000, P.R. China

[2]Department of Physiology, School of Basic Medical Science, Central South University, Changsha, Hunan Province 410000, P.R. China

[3]State Key Laboratory of Cellular Stress Biology, Innovation Center for Cell Signaling Network, School of Life Sciences, Xiamen University, Xiamen, Fujian, China

[4]Department of Respiratory Diseases and Critical Care Illness, The 3Road Xiangya Hospital, Central South University, Changsha 410000, P.R. China

[5]Hunan Key Laboratory of Organ Fibrosis, Xiangya Hospital, Central South University, Changsha 410000, P.R. China

[6]ICU Center, The Second Xiangya Hospital, Central South University, Changsha 410000, P.R. China

[7]Key Laboratory of Sepsis Translational Medicine of Hunan, Central South University, Changsha, Hunan Province 410000, P.R. China

[8]Department of Pathophysiology, School of Basic Medical Science, Central South University, Changsha, Hunan Province 410000, P.R. China

[9]The Feinstein Institute for Medical Research, Northwell Health, 350 Community Drive, Manhasset, NY 11030, USA

[10]Department of Surgery, University of Pittsburgh Medical Center, Pittsburgh, PA 15213, USA

[11]Lead contact

[12]These authors contributed equally

*Correspondence: xybenlu@csu.edu.cn (B.L.), liangfang924@163.com (F.L.)

https://doi.org/10.1016/j.isci.2022.104647

2019), partly by releasing proinflammatory cytokines (e.g., tumor necrosis factor) and profibrogenic factors (Li et al., 2016).

To investigate whether different immune states are critical for the susceptibility of silicosis, we performed single-cell RNA sequencing analysis of cells from bronchoalveolar lavage fluid (BALF) obtained from small-scale mine workers with or without silicosis. This led to the finding that the interferon (IFN)-γ signaling is significantly lacking in myeloid cells (e.g., macrophages and monocytes) from silicosis patients. The loss of IFN-γ signaling has long been considered as the key contributor of tumorigenesis and pathogen infection, but its role in environmental irritants-mediated diseases, especially silica crystal-mediated pulmonary fibrosis, is still unknown. Based on the scRNA results, we will establish a murine silicosis model on IFN-γ receptor (IFN-γR)-deficiency mice to explore the relationship between IFN-γ signaling deficiency and silicosis susceptibility, and further to explore whether IFN-γ signaling deficiency will lead to the activation of NLRP3 inflammasome in silicosis. As IFN-γ is a key player in both innate and adaptive immune responses, this research will extend our understanding of how the immune system regulates host responses to environmental irritants and suggest that IFNg signaling lacking-mediated immune suppression might be a high-risk factor for the development of silicosis.

RESULTS

Reduced IFN-γ signaling in myeloid cells was strongly associated with the occurrence of silicosis in mine workers

The problem of silicosis is particularly prevalent in workers in small-scale mines because of chronic inhalation of crystalline silica dust particles. Up to 20% of these workers have an accelerated form of the disease (Wang et al., 2020). To examine whether different immune states contributes to individual susceptibility to silicosis, we recruited patients with silicosis and sex-, age- and exposure time-matched co-workers without silicosis from small-scale coal mines in Hunan province, a region that has the highest silicosis incidence in the world. The diagnosis of silicosis was based on computed tomography (CT) (Figure 1A). The CT image of silicosis patients presented increased reticular markings and several nodule formations in the upper part of the lung when compared to the exposure miners (Figure 1A). Single-cell RNA sequencing analysis (scRNA-seq) was performed on cells from bronchoalveolar lavage fluid (BALF) (Figure 1B). Intriguingly, two distinct monocyte/macrophage subclusters (named as C1 and C2) were observed by an unbiased whole genome analysis in both silicosis patients and their disease-free co-workers. Although C2 was enriched in monocytes/macrophages from silicosis patients, cluster C1 was composed of cells predominantly from subjects without silicosis (Figures 1B and 1C). The heatmap listed the gene that was found to have the most striking difference in expression between the monocytes/macrophages from silicosis patients and disease-free mine workers (Figure 1D). The differentially expressed genes in the monocyte/macrophage population were analyzed to identify signaling pathways relevant to the occurrence of silicosis (Figure 1E). Among, IFN-γ signaling as one of the strikingly difference expression gene, had been confirmed to participate in vesicle transport, immune and inflammation process in many kinds of diseases(Ivashkiv,2018; Langer et al., 2019; Schnettger et al., 2017). Hence, we speculated that IFN-γ signaling plays a vital role in silicosis. Compared to control genes, genes associated with IFN-γ signaling were notably lower in cells from silicosis patients (Figures S1, 1E, and 1F). Monocytes/macrophages from silicosis patients hardly expressed IFN-γR1, IFN-γR2, STAT1, JAK2, IRF1, and IRF9, all of which are the key components of the IFN-γ pathway (Figure 1F). We confirmed this observation using real-time qPCR (Figure 1G). The development of silicosis correlates with progressive loss of lung function, which is characterized by a decrease in forced vital capacity (FVC), forced expiratory volume in 1 s (FEV1) and the ratio of FEV1 to FVC. To determine if loss of IFN-γ signaling genes was associated with respiratory dysfunction, we analyzed the correlation between the expression of IFN-γ signaling pathway components and lung function. IFN-γR1, IFN-γR2, STAT1, and JAK2 mRNA levels were significantly correlated with FEV1, FVC, and FEV1/FVC (Figures 1H–1K). Together, these observations establish that a failure to express IFN-γ signaling components in lung myeloid cells was strongly associated with the occurrence of silicosis.

Impaired IFN-γ signaling promotes silica crystals-induced pulmonary interstitial fibrosis and respiratory dysfunction

To test the functional relevance of impaired IFN-γ signaling to the development of silicosis, we utilized a murine silicosis model, in which wild-type (WT) mice and IFN-γ receptor (IFN-γR)-deficient mice were intratracheally injected with a silica crystal suspension. The degree of pulmonary interstitial fibrosis was visualized using micro-computed tomography. Intratracheal atomizing injection of silica crystals (200 mg/kg

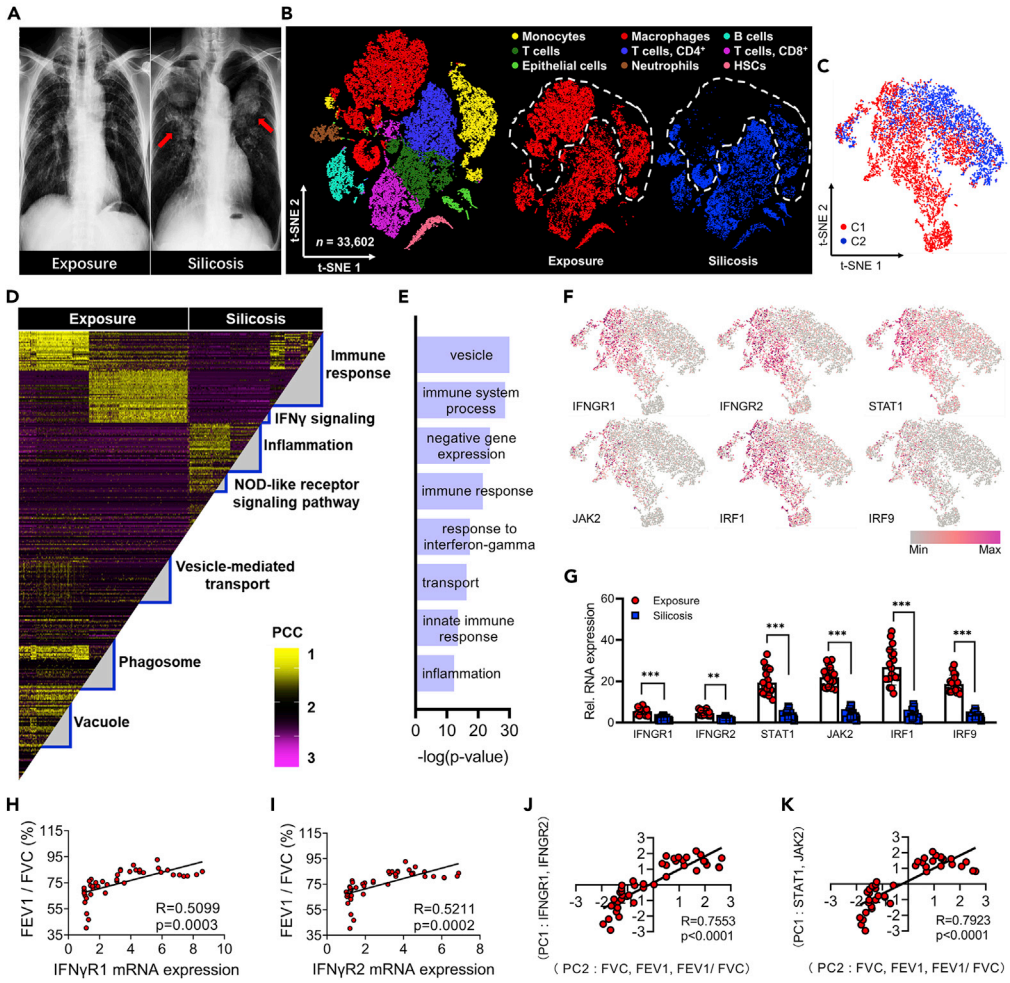

Figure 1. Reduced IFN-γ signaling in myeloid cells was strongly associated with the occurrence of silicosis in mine workers

(A) Representative images of pulmonary CT from exposure miner and silicosis patients. (Red arrow: several nodule).

(B) t-Distributed stochastic neighbor embedding (t-SNE) plot and density plots of 10,000 RNA-sequenced (RNA-seq) single cells from exposure miner and silicosis patient bronchoalveolar lavage fluid. (n = 2 biological replicates for exposure miners and n = 3 biological replicates for silicosis patients).

(C) The distinct subclusters of monocyte-macrophages derived by reference to the ImmGen database with clusters superimposed on the t-SNE plot.

(D) Heatmap of the expression of genes in bulk RNA-seq of monocyte-macrophages from bronchoalveolar lavage fluid cells of exposure miners and silicosis patients.

(E) Functional enrichment analysis with GO Biological Processes for monocyte-macrophages was performed using GOrilla with the significantly changed genes in silicosis patients compared to exposure miners.

(F) Feature plots demonstrating differential expression of selected alveolar monocyte-macrophage genes (IFNGR1, IFNGR2, STAT1, JAK2, IRF1, IRF9).

(G) The mRNA expression detected by qPCR in bronchoalveolar lavage fluid cells from exposure miners and silicosis patients. Data are represented as mean ± SEM (n = 19 for exposure miners and n = 23 for silicosis patients).

(H) The mRNA levels of IFNGR1 are significantly correlated with the lung function indexes (FEV1/FVC) in exposure miners and silicosis patients.

(I) The mRNA levels of IFNGR2 are significantly correlated with the lung function indexes (FEV1/FVC) in exposure miners and silicosis patients.

(J) Principal component analysis (PCA) of the correlation between IFN-γ signaling and lung function (PC1: IFNGR1 and IFNGR2; PC2: FVC, FEV1, FEV1/FVC).

(K) Principal component analysis (PCA) of the correlation between IFN-γ signaling and lung function (PC1: STAT1 and JAK2; PC2: FVC, FEV1, FEV1/FVC).

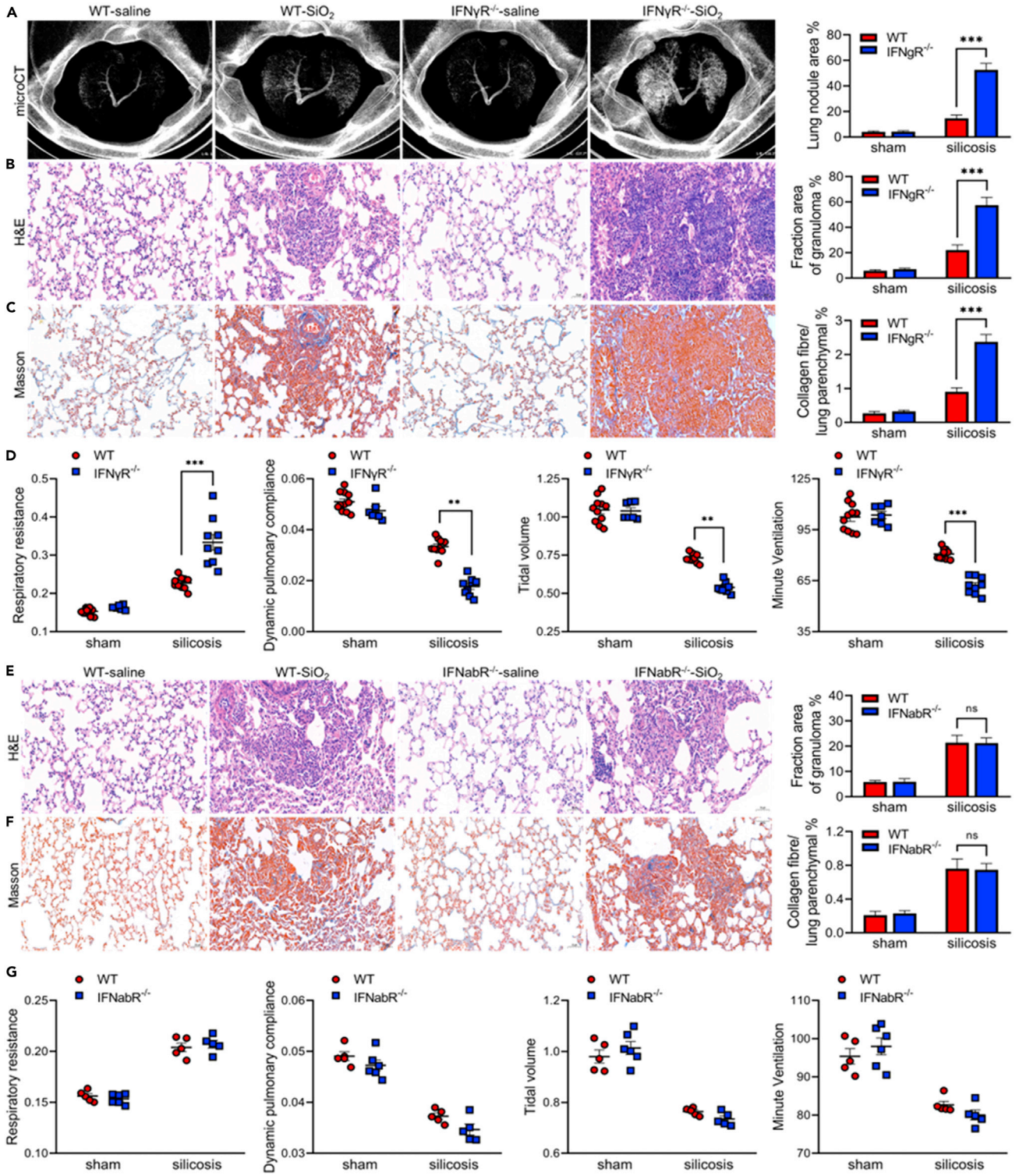

Figure 2. Impaired IFN-γ signaling promotes silica crystals-induced pulmonary interstitial fibrosis and respiratory dysfunction

(A). Lung nodule of lung tissues was observed by 2D reconstruction of lung microstructure in wild type or IFN-γR knockout mice inhaled with or without silica crystals. Morphometry analysis quantifying lung nodule area in the lungs. Data are represented as mean ± SEM (n = 11 for WT-saline, n = 10 for WT-SiO_2, n = 7 for IFNgR knockout-saline and n = 9 for IFNgR knockout-SiO_2).

Figure 2. *Continued*

(B) H&E staining of lung tissues in wild type or IFN-γR knockout mice presented with or without silica crystals. Morphometry analysis quantifying granuloma area in the lungs. Data are represented as mean ± SEM (n = 11 for WT-saline, n = 10 for WT-SiO_2, n = 7 for IFNgR knockout-saline and n = 9 for IFNgR knockout-SiO_2).

(C) Masson staining of lung tissues in wild type or IFN-γR knockout mice inhaled with or without silica crystals. Morphometry analysis quantifying collagen fiber area in the lungs. Data are represented as mean ± SEM (n = 11 for WT-saline, n = 10 for WT-SiO_2, n = 7 for IFNgR knockout-saline and n = 9 for IFNgR knockout-SiO_2).

(D) Wild type or IFN-γR knockout mice were subjected to lung function assessment. Resistance index (RI), dynamic compliance (Cdyn), tidal volume (TV) and minute volume (MV) were measured. Data are represented as mean ± SEM (n = 11 for WT-saline, n = 10 for WT-SiO_2, n = 7 for IFNgR knockout-saline and n = 9 for IFNgR knockout-SiO_2).

(E) H&E staining of lung tissues in wild type or IFNabR knockout mice inhaled with or without silica crystals. Morphometry analysis quantifying granuloma area in the lungs. Data are represented as mean ± SEM (n = 5).

(F) Masson staining of lung tissues in wild type or IFNabR knockout mice inhaled with or without silica crystals. Morphometry analysis quantifying Collagen fiber area in the lungs. Data are represented as mean ± SEM (n = 5).

(G) Wild type or IFNabR knockout mice were subjected to lung function assessment. Resistance index (RI), dynamic compliance (Cdyn), tidal volume (TV) and minute volume (MV) were measured. Data are represented as mean ± SEM (n = 5) *p < 0.05; **p < 0.01; ***p < 0.001; NS, no statistical difference (unpaired/two-tailed *t*-test, one-way and two-way ANOVA test). Data are shown as mean ± SEM of three independent experiments. Scale bar represents 5 μm.

mice) induced a severe pulmonary fibrosis in IFN-γR-deficient mice but only a mild fibrosis in WT controls (Figure 2A). As revealed by hematoxylin-eosin (H&E) and Masson staining, IFN-γR deficient mice exhibited many more contiguous fibrotic masses and air bubbles, and greater fibrous obliteration as compared to their WT controls (Figures 2B and 2C). Deletion of IFN-γR markedly promoted silica crystals-induced pulmonary interstitial fibrosis (Figure 2C). These changes were associated with a decrease in dynamic compliance (Cdyn), tidal volume (TV) and minute volume (MV), and significantly increased respiratory resistance index (RI) in IFN-γR deficient mice (Figure 2D). Unlike IFN-γ, type 1 IFNs such as IFN-α and IFN-β activate JAK pathway through their receptor IFNαbR (Ivashkiv and Donlin,2014). In contrast to IFN-γR deficiency, the loss of IFNαbR failed to affect silica crystals-induced pulmonary interstitial fibrosis and respiratory dysfunction in the murine silicosis model (Figures 2E–2G). Together, these findings demonstrate that the impaired IFN-γ signaling promotes silica crystals-induced pulmonary interstitial fibrosis and respiratory dysfunction, and establish a functional link between suppressed IFN-γ signaling and the susceptibility to silicosis.

Impaired IFN-γ signaling in myeloid cells promotes silica crystals-induced pulmonary interstitial fibrosis and respiratory dysfunction

Myeloid cells, such as macrophages and monocytes, express functional IFN-γR (Pietras et al., 2011). Numerous studies suggest that alveolar macrophages play critical roles in lung inflammation and pulmonary fibrosis, and are the major cells in the lungs that engulf inhaled crystalline silica (Dostert et al., 2008; Hornung et al., 2008). Thus, we next determined whether impaired IFN-γ signaling in myeloid cells drives the development and progression of silicosis. Mice with selective IFN-γR deletion in myeloid cells (*IFN-γR$^{f/f}$ Lyz2-cre^{+}*) were generated. These mice displayed no detectable defects under physiological conditions, and exhibited normal lung histology after intratracheal injection of saline vehicle control (Figure 3A). In the murine silicosis model, however, *IFN-γR$^{f/f}$ Lyz2-cre^{+}* mice exhibited many more contiguous fibrotic lung masses and more pronounced pulmonary interstitial fibrosis as compared to *IFN-γR$^{+/+}$ Lyz2-cre^{-}*, *IFN-γR $^{f/f}$ Lyz2-cre^{-}* or *IFN-γR $^{f/+}$ Lyz2-cre^{+}* mice that express IFN-γR in myeloid cells (Figures 3A–3C). In agreement with these findings, selective deletion of IFN-γR in myeloid cells markedly decreased dynamic compliance (Cdyn), tidal volume (TV) and minute volume (MV), and significantly increased respiratory resistance index (RI) following intratracheal injection of silica crystal suspension (Figure 3D). Collectively, these data indicate that impaired IFN-γ signaling in myeloid cells promotes silica crystals-induced pulmonary interstitial fibrosis and respiratory dysfunction.

Impaired IFN-γ signaling promotes silica crystals-induced pulmonary interstitial fibrosis and respiratory dysfunction through the NLRP3 inflammasome

Next, we investigated the mechanisms by which impaired IFN-γ signaling promotes pulmonary interstitial fibrosis and respiratory dysfunction in our model of silicosis. Because IL-1α、IL-1β、IL-17A、IL-23, IL-27, MCP-1, and IL-10 as important proinflammatory cytokines that significantly associated with the progression of silicosis(Liu et al., 2015; Cao et al., 2021; Chen et al., 2017; Luna-Gomes et al., 2015; Slavov et al., 2010), we measured these cytokine levels in the BALF using a Cytometric Bead Array. Inhalation of silica crystals increased the release of IL-1β, and to a lesser extent, IL-1α, whereas the BALF levels of IL-17A, IL-23, IL-27,

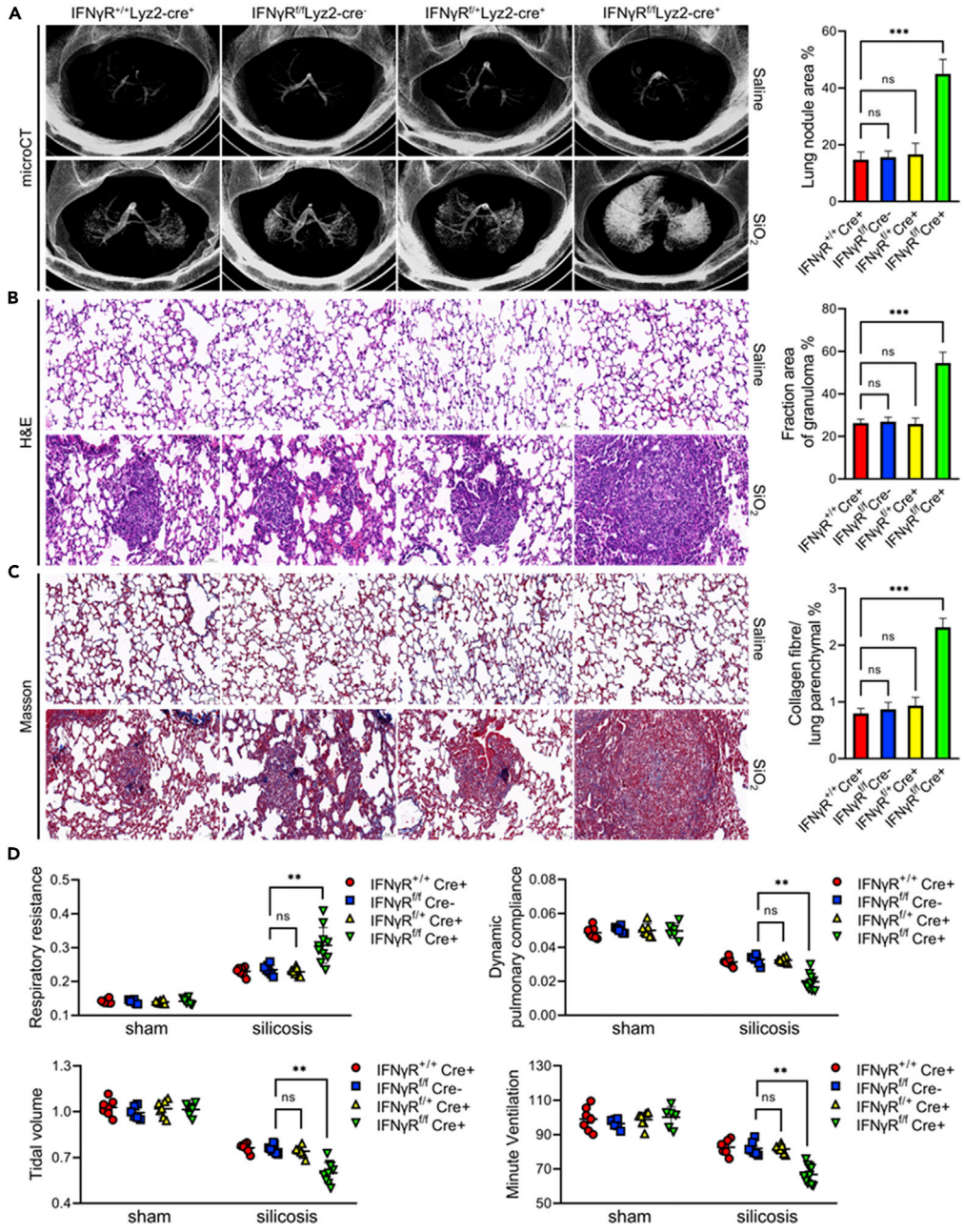

Figure 3. Impaired IFN-γ signaling in myeloid cells promotes silica crystals-induced pulmonary interstitial fibrosis and respiratory dysfunction

(A). Lung nodule of lung tissues was observed by 2D reconstruction of lung microstructure in IFN-γR$^{+/+}$ Cre^{+}, IFN-γR$^{f/f}$ Cre^{-}, IFN-γR$^{f/+}$ Cre^{+} and IFN-γR$^{f/f}$ Cre^{+} mice inhaled with or without silica crystals. Morphometry analysis quantifying lung nodule area in the lungs. Data are represented as mean ± SEM (n = 7 for IFN-γR$^{+/+}$ Cre^{+}- SiO_2, n = 7 for IFN-γR$^{f/f}$ Cre^{-}-SiO_2, n = 7 for IFN-γR$^{f/+}$ Cre^{+}- SiO_2 and n = 10 for IFN-γR$^{f/f}$ Cre^{+}-SiO_2).

(B) H&E staining of lung tissues in in IFN-γR$^{+/+}$ Cre^{+}, IFN-γR$^{f/f}$ Cre^{-}, IFN-γR$^{f/+}$ Cre^{+} and IFN-γR$^{f/f}$ Cre^{+} mice inhaled with or without silica crystals. Morphometry analysis quantifying granuloma area in the lungs. Data are represented as mean ± SEM (n = 7 for IFN-γR$^{+/+}$ Cre^{+}- SiO_2, n = 7 for IFN-γR$^{f/f}$ Cre^{-}-SiO_2, n = 7 for IFN-γR$^{f/+}$ Cre^{+}- SiO_2 and n = 10 for IFN-γR$^{f/f}$ Cre^{+}-SiO_2).

(C) Masson staining of lung tissues in IFN-γR$^{+/+}$ Cre^{+}, IFN-γR$^{f/f}$ Cre^{-}, IFN-γR$^{f/+}$ Cre^{+} and IFN-γR$^{f/f}$ Cre^{+} mice inhaled with or without silica crystals. Morphometry analysis quantifying collagen fiber area in the lungs. Data are represented as mean ± SEM (n = 7 for IFN-γR$^{+/+}$ Cre^{+}- SiO_2, n = 7 for IFN-γR$^{f/f}$ Cre^{-}-SiO_2, n = 7 for IFN-γR$^{f/+}$ Cre^{+}- SiO_2 and n = 10 for IFN-γR$^{f/f}$ Cre^{+}-SiO_2).

(D) IFN-γR$^{+/+}$ Cre^{+}, IFN-γR$^{f/f}$ Cre^{-}, IFN-γR$^{f/+}$ Cre^{+} and IFN-γR$^{f/f}$ Cre^{+} mice were subjected to lung function assessment. Resistance index (RI), dynamic compliance (Cdyn), tidal volume (TV) and minute volume (MV) were measured. Data are represented as mean ± SEM (n = 6–10) *p < 0.05; **p < 0.01; ***p < 0.001; NS, no statistical difference (unpaired/two-tailed *t*-test, one-way and two-way ANOVA test). Data are shown as mean ± SEM of three independent experiments. Scale bar represents 5 μm.

MCP-1 and IL-10 were not altered (Figure 4A). Previous findings have shown a pathogenic role of IL-1β in the development of silicosis. Notably, IFN-γR deficiency was associated with significantly higher concentrations of IL-1β and IL-1α in the BALF when compared to WT mice receiving intratracheal silica crystal suspension (Figure 4A). IL-1β and IL-1α exert biological functions through their receptor IL-1R. Deletion of IL-1R in IFN-γR deficient mice almost completely prevented silica crystals-induced pulmonary interstitial fibrosis and respiratory dysfunction (Figures 4B and 4C). In line with previous findings, silica crystals induce the release of IL-1β and pulmonary interstitial fibrosis through the NLRP3 inflammasomes (Hornung et al., 2008). Deletion of NLRP3 in IFN-γR deficient mice also blocked silica crystals-induced pulmonary interstitial fibrosis and respiratory dysfunction in a manner similar to that seen with IL-1R deletion (Figures 4D and 4E). These observations clearly suggest that IFN-γR deficiency promotes the activation of NLRP3 inflammasome upon crystalline silica stimulation.

To test this possibility, we incubated LPS-primed mouse macrophages isolated from WT or IFN-γR deficient mice with silica crystals in the presence or the absence of recombinant IFN-γ at physiological concentrations. Stimulation with IFN-γ markedly decreased silica crystals-induced release of IL-1β and cleavage of pro-caspase-1 in a NLRP3-dependent manner in WT but not IFN-γR deficient macrophages (Figures 4F and 4G) (L = LPS, IL = IFNγ + LPS, LSi = LPS + SiO_2 and ILSi = IFNγ + LPS + SiO_2). Intriguingly, deletion of IFN-γR slightly increased IL-1β release and caspase-1 cleavage even in the absence of recombinant IFN-γ (Figures 4F and 4G). We further tested whether IFN-γ is a broad-spectrum inhibitor of inflammasome activation. LPS-primed WT macrophages were stimulated with ATP, nigericin, or monosodium urate (MSU) to induce NLRP3-dependent inflammasome activation. Macrophages were also transfected with either poly(dA:dT) or flagellin (FLA) to activate the AIM2 inflammasome or the NLRC4 inflammasome, respectively. In line with previous findings (Shenoy et al., 2012), priming with IFN-γ enhanced ATP- and nigericin-induced IL-1β release but failed to affect MSU-, poly(dA:dT)- or FLA-induced IL-1β release (Figure 4H). Addition of IFN-γ significantly increased *E. coli*-induced IL-1β release (Figure 4I), which depends on the caspase-11 non-canonical inflammasome (Kayagaki et al., 2015). Although IFN-α or IFN-β could broadly inhibit the NLRP3 inflammasome activation when given at extremely high concentrations (Guarda et al., 2011), they did not affect NLRP3 inflammasome activation at physiological concentrations (Figure 4J). Together, these findings indicate that IFN-γ signaling counter-regulates the silica crystals-induced NLRP3 inflammasome activation.

IFN-γ signaling inhibits silica crystals-induced NLRP3 inflammasome activation by preventing lysosomal rupture

Interestingly, IFN-γ priming significantly inhibited adjuvant aluminum-induced IL-1β release (Figure S2). This observation is in line with a previous study showing that adjuvant aluminum is unable to induce robust IL-1β release in IFN-γ + lipopolysaccharide-primed macrophages (Shenoy et al., 2012). Unlike other NLRP3 stimuli, both silica crystals and adjuvant aluminum are able to trigger lysosomal rupture (Hornung et al., 2008), which activates the NLRP3 inflammasome through potassium efflux (Hornung et al., 2008; Munoz-Planillo et al., 2013). To confirm that priming with IFN-γ prevents silica crystals-induced lysosomal rupture, we isolated the cytosolic fraction of macrophages and measured the quantity of cathepsin D, a lysosomal protease. Priming with IFN-γ prevented the appearance of cathepsin D in the cytoplasmic compartment in silica crystals-stimulated WT but not IFN-γR deficient macrophages (Figure 5A). Next, we used acridine orange to quantitatively measure lysosomal integrity and found that IFN-γ concentration-dependently inhibited silica crystals-induced lysosomal damage in WT but not IFN-γR-deficient macrophages (Figure 5B). To provide further evidence that IFN-γ inhibits silica crystals-induced NLRP3 inflammasome activation by preventing lysosomal rupture, WT and IFN-γR-deficient macrophages were incubated with L-leucyl-L-leucine methyl ester (Leu-Leu-OMe), a functionalized dipeptide that disrupts lysosomes when converted to a membranolytic compound by the lysosomal enzyme dipeptidylpeptidase I in the lysosomes (Bonet-Ponce et al., 2020; Hornung et al., 2008). Priming with IFN-γ prevented Leu-Leu-OMe-induced lysosomal damage and leakage of cathepsin D to the cytosol (Figures 5C and 5D). Accordingly, IFN-γ markedly inhibited Leu-Leu-OMe-induced IL-1β release and caspase-1 cleavage in WT but not IFN-γR deficient

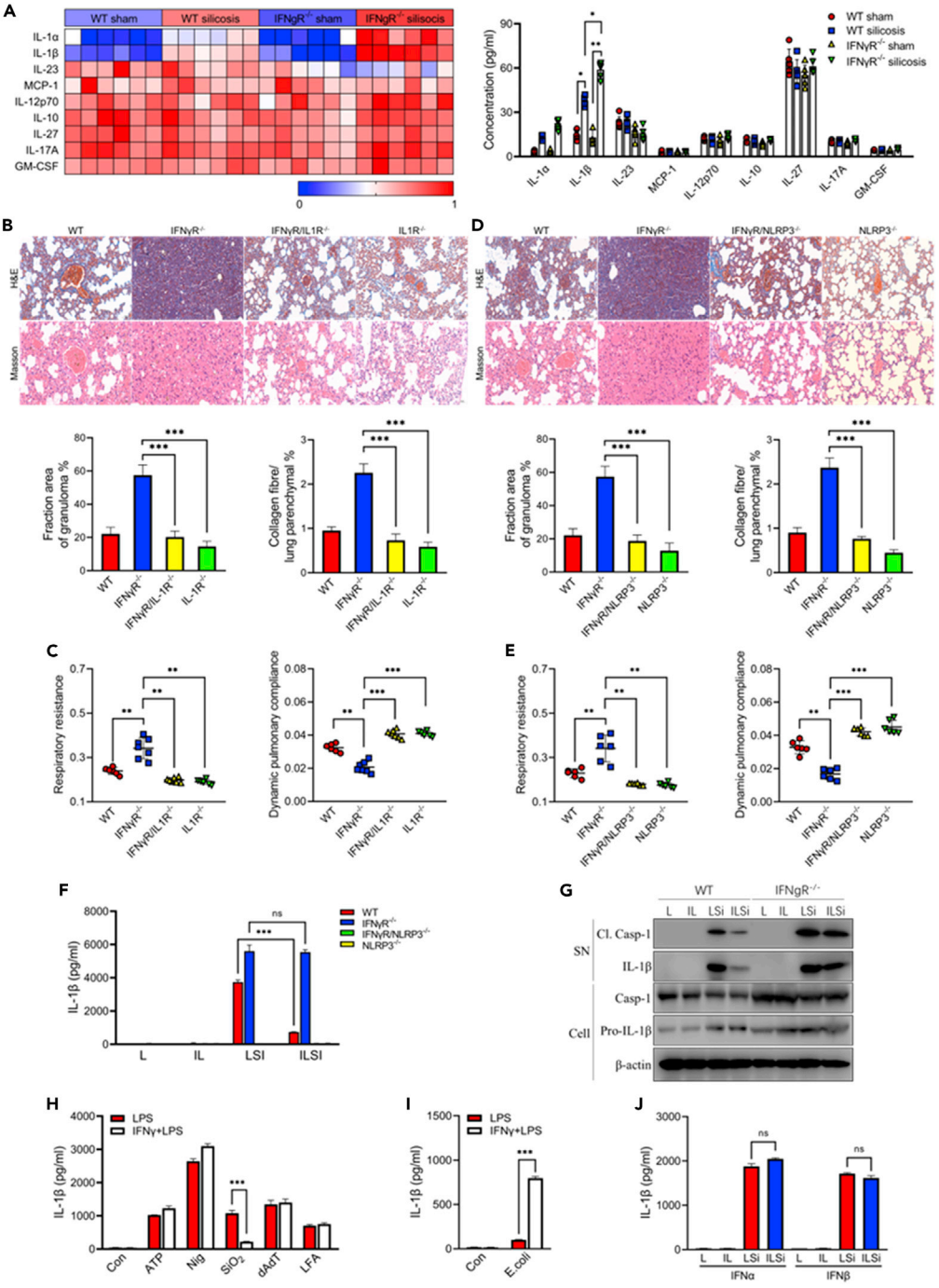

Figure 4. Impaired IFN-γ signaling promotes silica crystals-induced pulmonary interstitial fibrosis and respiratory dysfunction through the NLRP3 inflammasome

(A) Heatmap and statistical data of cytokine levels in bronchoalveolar lavage fluid cells of wild type or IFN-γ knockout mice presented with or without silica crystals. Data are represented as mean ± SEM.

(B) Masson and H&E staining of lung tissues in wild type, IFN-γR$^{-/-}$, IFN-γR/IL1R$^{-/-}$ and IL1R$^{-/-}$ mice presented with silica crystals. Morphometry analysis quantifying fibrosis degree in the lungs. Data are represented as mean ± SEM (n = 6 for Wild type-SiO_2, n = 7 for IFN-γR$^{-/-}$-SiO_2, n = 7 for IFN-γR/IL1R$^{-/-}$- SiO_2 and n = 6 for IL1R$^{-/-}$-SiO_2).

(C) Wild type, IFN-γR$^{-/-}$, IFN-γR/IL1R$^{-/-}$and IL1R$^{-/-}$ mice were subjected to lung function assessment. Resistance index (RI) and dynamic compliance (Cdyn) were measured. Data are represented as mean ± SEM (n = 6 for Wild type-SiO_2, n = 7 for IFN-γR$^{-/-}$-SiO_2, n = 7 for IFN-γR/IL1R$^{-/-}$- SiO_2 and n = 6 for IL1R$^{-/-}$-SiO_2).

Figure 4. *Continued*

(D) Masson and H&E staining of lung tissues in wild type, IFN-γR$^{-/-}$, IFN-γR/NLRP3$^{-/-}$ and NLRP3$^{-/-}$ mice presented with silica crystals. Morphometry analysis quantifying fibrosis degree in the lungs. Data are represented as mean ± SEM (n = 6 for Wild type-SiO_2, n = 7 for IFN-γR$^{-/-}$-SiO_2, n = 7 for IFN-γR/IL1R$^{-/-}$- SiO_2 and n = 6 for IL1R$^{-/-}$-SiO_2).

(E) Wild type, IFN-γR$^{-/-}$, IFN-γR/NLRP3$^{-/-}$and NLRP3$^{-/-}$ mice were subjected to lung function assessment. Resistance index (RI) and dynamic compliance (Cdyn) were measured. Data are represented as mean ± SEM (n = 6 for Wild type-SiO_2, n = 7 for IFN-γR$^{-/-}$-SiO_2, n = 7 for IFN-γR/IL1R$^{-/-}$- SiO_2 and n = 6 for IL1R$^{-/-}$-SiO_2).

(F) IL-1β secretion in wild type, IFN-γR$^{-/-}$, IFN-γR/IL1R$^{-/-}$, IL1R$^{-/-}$, IFN-γR/NLRP3$^{-/-}$ and NLRP3$^{-/-}$ peritoneal macrophages stimulated with SiO_2 after LPS or LPS + IFN-γ priming. Data are represented as mean ± SEM.

(G) Immunoblotting for IL-1β, caspase-1, NLRP3, and β-actin in the supernatants (SN) or cell lysates (cell) of wild type and IFN-γR$^{-/-}$ mouse peritoneal macrophages stimulated with SiO_2 after LPS or LPS + IFN-γ priming.

(H) IL-1β secretion in wild type peritoneal macrophages stimulated with ATP, nigericin, SiO_2, dAdT or FLA after LPS or LPS + IFN-γ priming. Data are represented as mean ± SEM.

(I) IL-1β secretion in wild type peritoneal macrophages stimulated with *E. coli* after LPS or LPS + IFN-γ priming. Data are represented as mean ± SEM.

(J) IL-1β secretion in wild type peritoneal macrophages stimulated with SiO_2 after LPS, LPS + IFNα or LPS + IFNβ priming. Data are represented as mean ± SEM (L = LPS, I = IFNγ, Si = SiO_2)*p < 0.05; **p < 0.01; ***p < 0.001; NS, no statistical difference (unpaired/two-tailed *t*-test, one-way and two-way ANOVA test). Data are shown as mean ± SEM of three independent experiments. Scale bar represents 50 μm.

macrophages (Figures 5E and 5F). Taken together, these findings indicate that the IFN-γ signaling inhibits silica crystals-induced NLRP3 inflammasome activation by preventing lysosomal rupture.

IFN-γ signaling generates spacious phagosomes and reduces the ratio of silica crystal/phagosomal area

We next investigated the mechanisms by which IFN-γ signaling prevents silica crystals-induced lysosomal damage. As shown by both flow cytometry and fluorescent microscopy, IFN-γ stimulation did not affect the phagocytosis of Alex594-labeled silica crystals in macrophages (Figures 6A and 6B). To explore how IFN-γ signaling protects lysosomal membranes, WT and IFN-γR deficient macrophages were stimulated with silica crystals in the presence or the absence of IFN-γ and then subjected to transmission electron microscope (TEM) analysis. We observed that priming with IFN-γ generated much more spacious phagosomes and markedly decreased the ratio calculated as silica crystals/phagosomal area in WT but not IFN-γR deficient macrophages (Figures 6C–6E). To provide evidence to support the conclusion that reducing the contact between silica crystals and phagocytic membrane inhibits silica inhibits lysosomal damage and IL-1β release, the silica crystals were encapsulated in liposomes to reduce its direct contact with phagosomal membranes(Bollhorst et al., 2017) (Figures 7A and 7B). As revealed by acridine orange staining, encapsulation of silica crystals by liposomes markedly reduced the lysosomal damage and IL-1β release (Figures 7C and 7D). Importantly, priming with IFN-γ did not further reduce liposome-coated silica crystals-induced lysosomal damage and IL-1β release (Figures 7C and 7D). Together, these observations may suggest that IFN-γ signaling reduces the contact between crystalline silica and lysosomal membranes and thereby protects silica crystals-induced lysosomal membrane damage.

DISCUSSION

This work establishes the critical role of IFN-γ signaling in preventing crystalline silica-induced inflammatory responses and pulmonary interstitial fibrosis, a process resembling the immunopathology of clinical silicosis. IFN-γ, the sole type-II IFN, can be secreted by several types of immune cells (e.g., T lymphocytes and Natural killer cells) and functions as an activator for macrophages (Su et al., 2015). Activating IFN-γ signaling increases direct antimicrobial and antitumor activity and promotes antigen presentation (Baer et al., 2016; Kammertoens et al., 2017; Karki et al., 2021; Kerner et al., 2020). IFN-γ enhances the activation of caspase-11 (human caspase-4) and NLRP3 inflammasome through its downstream factors, such as guanylate-binding proteins and IRGB10 (Man et al., 2016; Meunier et al., 2014; Shenoy et al., 2012). These interferon-γ-inducible proteins directly target intracellular bacteria by assembling into a multi-protein platform that liberates pathogen ligands for immune detection (Man et al., 2016; Wandel et al., 2020). In the present study, however, we demonstrate an inhibitory role of IFN-γ signaling in NLRP3-dependent inflammatory responses induced by silica crystals, adjuvant aluminum and perhaps other types of crystals that are capable of destabilizing lysosomes. As IFN-γ is a key component in both innate and adaptive immunity, our findings provide insights into how the immune system regulates host responses to environmental irritants.

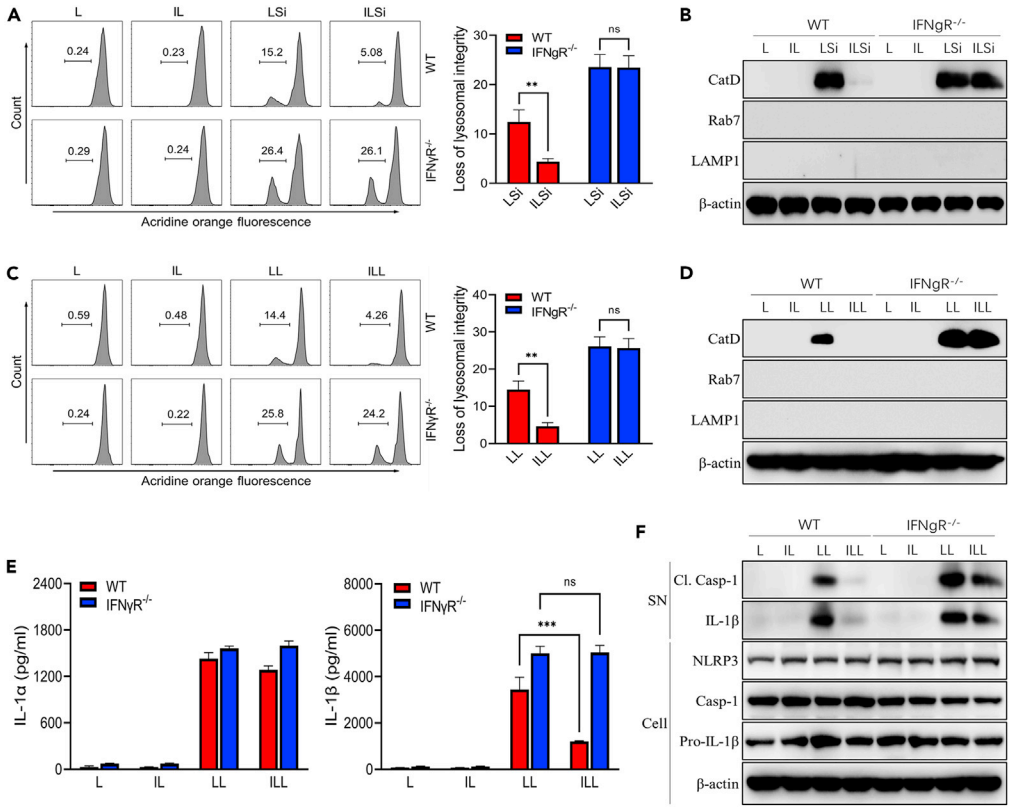

Figure 5. IFN-γ signaling inhibits silica crystals-induced NLRP3 inflammasome activation by preventing lysosomal rupture

(A) Flow cytometry of wild type and IFN-γR$^{-/-}$ mouse peritoneal macrophages stained with acridine orange and then treated with SiO_2 after LPS or LPS + IFN-γ priming. Data are represented as mean ± SEM.

(B) Immunoblotting for Cathepsin D, Rab7, Lamp1, and β-actin in the cytosolic fraction from wild type and IFN-γR$^{-/-}$ mouse peritoneal macrophages stimulated with SiO_2 after LPS or LPS + IFN-γ priming.

(C) Flow cytometry of wild type and IFN-γR$^{-/-}$ mouse peritoneal macrophages stained with acridine orange and then treated with Leu-Leu-OMe after LPS or LPS + IFN-γ priming. Data are represented as mean ± SEM.

(D) Immunoblotting for Cathepsin D, Rab7, Lamp1, and β-actin in the cytosolic fraction from wild type and IFN-γR$^{-/-}$ mouse peritoneal macrophages stimulated with Leu-Leu-OMe after LPS or LPS + IFN-γ priming.

(E) IL-1α and IL-1β secretion in wild type and IFN-γR$^{-/-}$ mouse peritoneal macrophages stimulated with Leu-Leu-OMe after LPS or LPS + IFN-γ priming. Data are represented as mean ± SEM.

(F) Immunoblotting for IL-1β, caspase-1, NLRP3, and β-actin in the supernatants (SN) or cell lysates (cell) of wild type and IFN-γR$^{-/-}$ mouse peritoneal macrophages stimulated with Leu-Leu-OMe after LPS or LPS + IFN-γ priming. (L = LPS, I = IFNγ, Si = SiO_2). *$p < 0.05$; **$p < 0.01$; ***$p < 0.001$; NS, no statistical difference (unpaired/two-tailed *t*-test, one-way and two-way ANOVA test). Data are shown as mean ± SEM of three independent experiments.

Though IFN-γ signaling does not affect the phagocytosis of silica crystals by macrophages, IFN-γ stimulation generates spacious phagosomes and thereby reduces the ratio of silica crystals/phagosomal area. Presumably, this process significantly decreases the frequency of contact between silica crystals and phagosomal membranes, and thereby preserves the integrity of silica crystals-containing phagosomes. However, we still need to further prove this conclusion because of the potential gene expression and cell function difference between peritoneal macrophages and bronchoalveolar alveolar lavage fluid macrophages.

Not only do humans inhale environmental irritants under hazardous working conditions or as the result of air-pollution but also lower species of animals (e.g., subterranean mammals) during evolution. It is likely that the IFN-γ signaling has offered protection against both environmental irritants and invading pathogens. During *Mycobacterium tuberculosis* (Mtb) infection, IFN-γ preserves the Mtb phagosome integrity for efficient pathogen elimination (Schnettger et al., 2017). As IFN-γ is a key cytokine for host immune

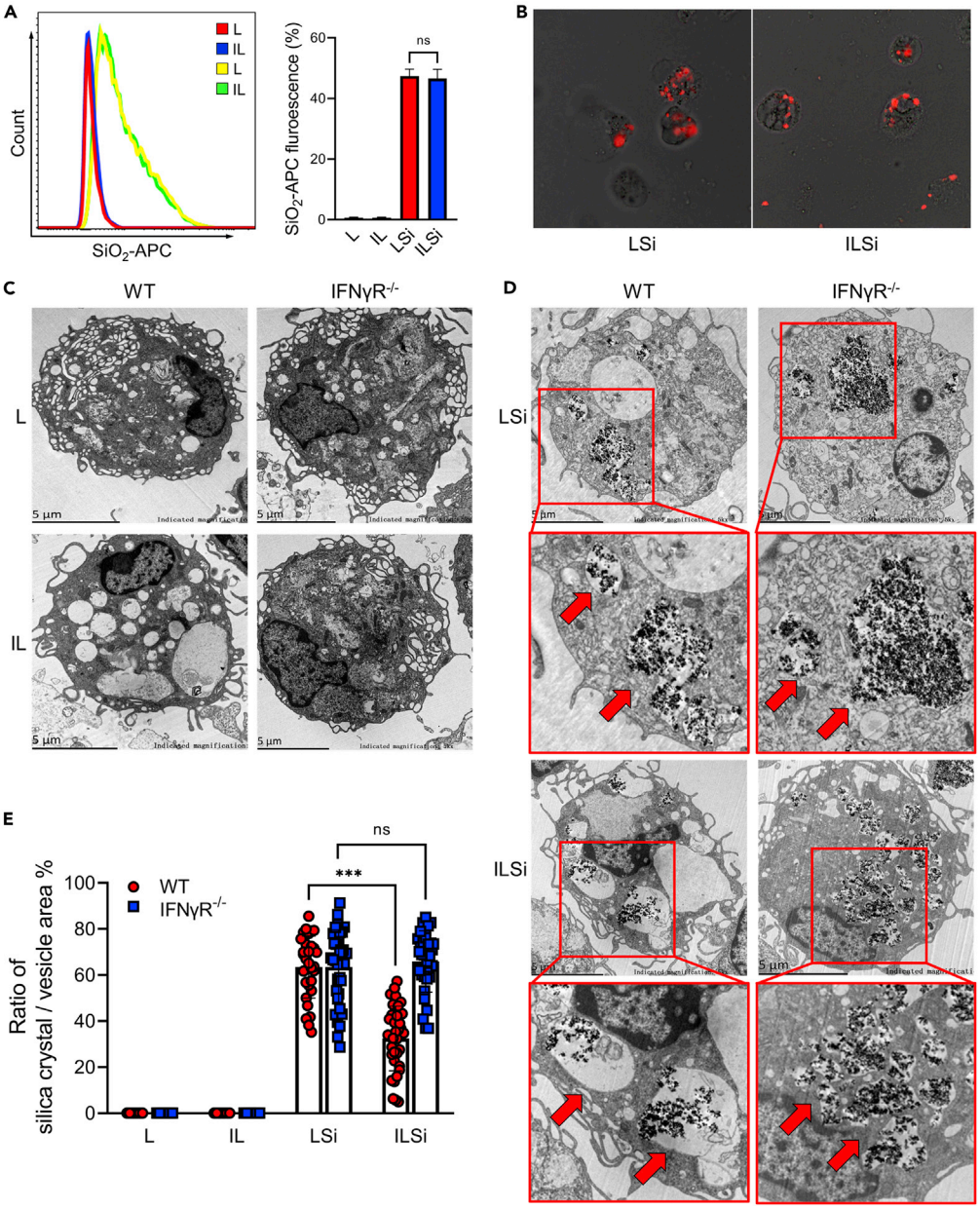

Figure 6. IFN-γ signaling generates spacious phagosomes and reduces the ratio of silica crystals/phagosomal area

(A) The Alex594 fluorescence intensity of wild type and IFN-γR$^{-/-}$ mouse peritoneal macrophages stimulated with Alex594-binding SiO_2 after LPS or LPS + IFN-γ priming. Data are represented as mean ± SEM.

(B) Confocal microscopy of wild type mouse peritoneal macrophages stimulated with Alex594-binding SiO_2 after LPS or LPS + IFN-γ priming.

(C) Representative TEM images of wild type and IFN-γR$^{-/-}$ mouse peritoneal macrophages primed with LPS or LPS + IFN-γ.

(D) Representative TEM images of wild type and IFN-γR$^{-/-}$ mouse peritoneal macrophages stimulated with SiO_2 after LPS or LPS + IFN-γ priming.

(E) The statistical data of the ratio of silica crystal/phagocytic vesicle area in wild type and IFN-γR$^{-/-}$ mouse peritoneal macrophages stimulated with SiO_2 after LPS or LPS + IFN-γ priming. Data are represented as mean ± SEM(L = LPS, I = IFNγ, Si = SiO_2) *$p < 0.05$; **$p < 0.01$; ***$p < 0.001$; NS, no statistical difference (unpaired/two-tailed *t*-test, one-way and two-way ANOVA test). Data are shown as mean ± SEM of three independent experiments. Scale bar represents 5 μm.

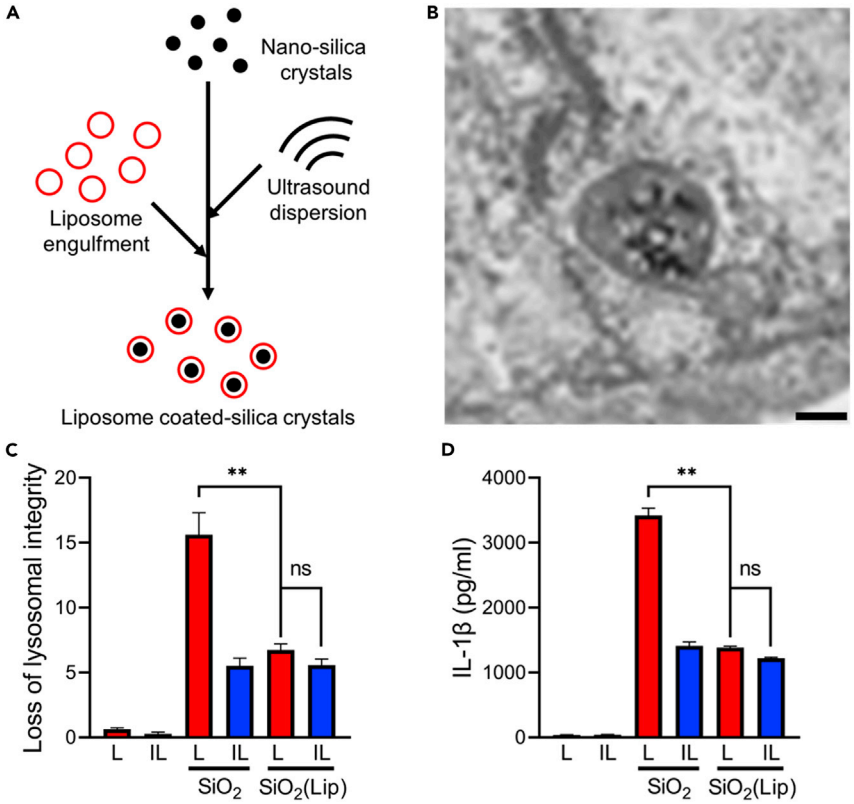

Figure 7. Reducing the contact between phagocytic membrane and silica crystals inhibits silica crystal-induced lysosomal rupture and IL-1β release

(A) The diagram of liposome-coated silica crystals.

(B) Representative TEM images of liposome-coated silica crystals in the phagosomes of wild-type mouse peritoneal macrophages.

(C) Flow cytometry of wild-type and IFN-γR$^{-/-}$ mouse peritoneal macrophages stained with acridine orange and then treated with silica crystals (SiO_2) after LPS or LPS + IFN-γ priming. Data are represented as mean ± SEM.

(D) IL-1β secretion from wild-type or IFN-γR$^{-/-}$ mouse peritoneal macrophages stimulated with Leu-Leu-OMe after LPS or LPS + IFN-γ priming. Data are represented as mean ± SEM(L = LPS, I = IFN-γ) **$p < 0.01$; NS, no statistical difference (one-way and two-way ANOVA test). Data are shown as mean ± SEM of three independent experiments. Scale bar represents 5 μm.

defense against Mtb infection, our finding that impaired IFN-γ signaling promotes the development of silicosis provides an explanation for the previously unsolved mystery of why tuberculosis risk is associated with severity of silicosis.

Though many preventive efforts have been made over the decades, silicosis remains one of the most important occupational diseases worldwide, particularly in countries of low- and middle-income (Knight et al., 2015; Leung et al., 2012). As only a small proportion of workers exposed to inhaled crystalline silica dusts eventually develop silicosis, identification of risk factors for disease susceptibility is of great importance. In addition to gene polymorphisms, measuring the gene expression signature for IFN-γ signaling in immune cells might be useful to identify workers who have high risks of developing silicosis. It is important to note that another strategy to prevent this occupational disease is to boost host immune responses with enhanced IFN-γ production, especially for those with immune suppression. But excessive increase of IFN-γ level also can trigger inflammation and tissue damage (Langer et al., 2019). Adjuvants or immunotherapeutic agents that promote T lymphocyte proliferation and activation could be suitable options to obtain normally physiological IFN-γ levels. Interestingly, thymosin alpha 1, a naturally occurring polypeptide with an excellent safety profile in the clinic, significantly attenuates disease severity in murine model of cystic fibrosis, a genetic disease lung fibrosis (Wandel et al., 2020). In addition, thymosin alpha 1 has been proved to promote the IFN-γ production in the respiratory tract of pulmonary tuberculosis patients (Wu

et al., 2022). But whether thymosin alpha 1 administration could prevent the development of silicosis in workers with inhaled crystalline silica exposure merits future studies. Taken together, this study provides a link between immune suppression and susceptibility of silicosis with implications for the prevention of this occupational disease.

Limitations of the study

We demonstrated that IFN-γ signaling plays an important protective role in silicosis patients, mouse silicosis models and *in vitro* systems. But the different sources of macrophage that were used in our study may limit the mechanism research of follow-up study. Performing *in vitro* study in bronchoalveolar alveolar lavage fluid macrophages is a better choice. And whether maintaining a normal physiological IFNg levels in minors can effectively inhibit the development of silicosis still needs further study.

STAR★METHODS

Detailed methods are provided in the online version of this paper and include the following:

- KEY RESOURCES TABLE
- RESOURCE AVAILABILITY
  - Lead contact
  - Materials availability
  - Data and code availability
- EXPERIMENTAL MODEL AND SUBJECT DETAILS
  - Clinical human samples
  - Mouse studies
  - Macrophage preparation and stimulation
- METHOD DETAILS
  - Analysis of bronchoalveolar lavage fluid cells by single cell RNA-seq
  - Fluorescent labeled silica nanoparticles
  - Silica crystals and liposome-coated silica crystals
  - Silicosis model
  - Macrophage stimulation
  - Micro-CT imaging
  - Lung function
  - H&E and masson staining
  - Cytometric Bead Array
  - ELISA
  - Immunoblotting
  - Flow cytometry
  - Quantification of silica crystals/phagosomal area
- QUANTIFICATION AND STATISTICAL ANALYSIS

SUPPLEMENTAL INFORMATION

Supplemental information can be found online at https://doi.org/10.1016/j.isci.2022.104647.

ACKNOWLEDGMENTS

We thank Fangfang Yuan and Xiangyu Wang for her excellent technical support. We thank Qianqian Xue and Ling Li for managing mouse colonies and research assistance. This work was supported by National Natural Science Foundation of China (No. 81700127, F.L.; No. 82025021, B.L.; No. 81930059, B.L.), Natural Science Foundation of Hunan Province (No. 2020JJ5860, F.L. and No. 2020JJ5864, Z.P.) and Innovation-driven scientific project of CSU (No.2019CX013, B.L.). The Fundamental Research Funds for the Central Universities of Central South University 2021zzts0402 and the Hunan Provincial Innovation Foundation for Postgraduate CX20210374.

AUTHOR CONTRIBUTIONS

B.L. conceived the project and designed experiments and wrote the paper. F.L. and Z.P. supervised the study, designed experiments, performed the experiments, and analyzed the data. M.D., Y.T., J.W., and

K.Z. performed the experiments. Z.H., J.M., F.C., X.X., and T.R.B assisted in data interpretation and edited the manuscript.

DECLARATION OF INTERESTS

The authors declare no competing interests.

Received: February 22, 2022
Revised: May 18, 2022
Accepted: June 15, 2022
Published: July 15, 2022

REFERENCES

Baer, C., Squadrito, M.L., Laoui, D., Thompson, D., Hansen, S.K., Kiialainen, A., Hoves, S., Ries, C.H., Ooi, C., and De Palma, M. (2016). Suppression of microRNA activity amplifies IFN-γ-induced macrophage activation and promotes anti-tumour immunity. Nat. Cell. Biol. *18*, 790–802. https://doi.org/10.1038/ncb3371.

Benmerzoug, S., Rose, S., Bounab, B., Gosset, D., Duneau, L., Chenuet, P., Mollet, L., Le Bert, M., Lambers, C., Geleff, S., et al. (2018). STING-dependent sensing of self-DNA drives silica-induced lung inflammation. Nat. Commun. *9*, 5226. https://doi.org/10.1038/s41467-018-07425-1.

Bollhorst, T., Rezwan, K., and Maas, M. (2017). Colloidal capsules: nano- and microcapsules with colloidal particle shells. Chem. Soc. Rev. *46*, 2091–2126. https://doi.org/10.1039/c6cs00632a.

Bonet-Ponce, L., Beilina, A., Williamson, C.D., Lindberg, E., Kluss, J.H., Saez-Atienzar, S., Landeck, N., Kumaran, R., Mamais, A., Bleck, C.K.E., et al. (2020). LRRK2 mediates tubulation and vesicle sorting from lysosomes. Sci. Adv. *6*, eabb2454. https://doi.org/10.1126/sciadv.abb2454.

Cao, Z., Song, M., Liu, Y., Pang, J., Li, Z., Qi, X., Shu, T., Li, B., Wei, D., Chen, J., et al. (2020). A novel pathophysiological classification of silicosis models provides some new insights into the progression of the disease. Ecotoxicol. Environ. Saf. *202*, 110834. https://doi.org/10.1016/j.ecoenv.2020.110834.

Cao, Z.J., Liu, Y., Zhang, Z., Yang, P.R., Li, Z.G., Song, M.Y., Qi, X.M., Han, Z.F., Pang, J.L., Li, B.C., et al. (2021). Pirfenidone ameliorates silica-induced lung inflammation and fibrosis in mice by inhibiting the secretion of interleukin-17A. Acta. Pharmacol. Sin. 908–918. https://doi.org/10.1038/s41401-021-00706-4.

Casey, M.L., and Mazurek, J.M. (2019). Silicosis prevalence and incidence among Medicare beneficiaries. Am. J. Ind. Med. *62*, 183–191. https://doi.org/10.1002/ajim.22944.

Cassel, S.L., Eisenbarth, S.C., Iyer, S.S., Sadler, J.J., Colegio, O.R., Tephly, L.A., Carter, A.B., Rothman, P.B., Flavell, R.A., and Sutterwala, F.S. (2008). The Nalp3 inflammasome is essential for the development of silicosis. Proc. Natl. Acad. Sci. *105*, 9035–9040. https://doi.org/10.1073/pnas.0803933105.

Chen, Y., Li, C., Lu, Y., Zhuang, H., Gu, W., Liu, B., Liu, F., Sun, J., Yan, B., Weng, D., and Chen, J. (2017). IL-10-Producing CD1d(hi)CD5(+) regulatory B cells may play a critical role in modulating immune homeostasis in silicosis patients. Front. Immunol. *8*, 110. https://doi.org/10.3389/fimmu.2017.00110.

Cullinan, P., Muñoz, X., Suojalehto, H., Agius, R., Jindal, S., Sigsgaard, T., Blomberg, A., Charpin, D., Annesi-Maesano, I., Gulati, M., et al. (2017). Occupational lung diseases: from old and novel exposures to effective preventive strategies. Lancet Respir. Med. *5*, 445–455. https://doi.org/10.1016/S2213-2600(16)30424-6.

Dostert, C., Petrilli, V., Van Bruggen, R., Steele, C., Mossman, B.T., and Tschopp, J. (2008). Innate immune activation through Nalp3 inflammasome sensing of asbestos and silica. Science *320*, 674–677. https://doi.org/10.1126/science.1156995.

Fernández Álvarez, R., Martínez González, C., Quero Martínez, A., Blanco Pérez, J.J., Carazo Fernández, L., and Prieto Fernández, A. (2015). Guidelines for the diagnosis and monitoring of silicosis. Arch. Bronconeumol. *51*, 86–93. https://doi.org/10.1016/j.arbres.2014.07.010.

Guarda, G., Braun, M., Staehli, F., Tardivel, A., Mattmann, C., Förster, I., Farlik, M., Decker, T., Du Pasquier, R.A., Romero, P., and Tschopp, J. (2011). Type I interferon inhibits interleukin-1 production and inflammasome activation. Immunity *34*, 213–223. https://doi.org/10.1016/j.immuni.2011.02.006.

Hornung, V., Bauernfeind, F., Halle, A., Samstad, E.O., Kono, H., Rock, K.L., Fitzgerald, K.A., and Latz, E. (2008). Silica crystals and aluminum salts activate the NALP3 inflammasome through phagosomal destabilization. Nat. Immunol. *9*, 847–856. https://doi.org/10.1038/ni.1631.

Ivashkiv, L.B. (2018). IFNγ: signalling, epigenetics and roles in immunity, metabolism, disease and cancer immunotherapy. Nat. Rev. Immunol. *18*, 545–558. https://doi.org/10.1038/s41577-018-0029-z.

Ivashkiv, L.B., and Donlin, L.T. (2014). Regulation of type I interferon responses. Nat. Rev. Immunol. *14*, 36–49. https://doi.org/10.1038/nri3581.

Kammertoens, T., Friese, C., Arina, A., Idel, C., Briesemeister, D., Rothe, M., Ivanov, A., Szymborska, A., Patone, G., Kunz, S., et al. (2017). Tumour ischaemia by interferon-gamma resembles physiological blood vessel regression. Nature *545*, 98–102. https://doi.org/10.1038/nature22311.

Karki, R., Sharma, B.R., Tuladhar, S., Williams, E.P., Zalduondo, L., Samir, P., Zheng, M., Sundaram, B., Banoth, B., Malireddi, R.S., et al. (2021). Synergism of TNF-α and IFN-γ triggers inflammatory cell death, tissue damage, and mortality in SARS-CoV-2 infection and cytokine shock syndromes. Cell *184*, 149–168.e17. https://doi.org/10.1016/j.cell.2020.11.025.

Kayagaki, N., Stowe, I.B., Lee, B.L., O Rourke, K., Anderson, K., Warming, S., Cuellar, T., Haley, B., Roose-Girma, M., Phung, Q.T., et al. (2015). Caspase-11 cleaves gasdermin D for non-canonical inflammasome signalling. Nature *526*, 666–671. https://doi.org/10.1038/nature15541.

Kerner, G., Rosain, J., Guérin, A., Al-Khabaz, A., Oleaga-Quintas, C., Rapaport, F., Massaad, M.J., Ding, J.Y., Khan, T., Ali, F.A., et al. (2020). Inherited human IFN-γ deficiency underlies mycobacterial disease. J. Clin. Invest. *130*, 3158–3171. https://doi.org/10.1172/JCI135460.

Knight, D., Ehrlich, R., Fielding, K., Jeffery, H., Grant, A., and Churchyard, G. (2015). Trends in silicosis prevalence and the healthy worker effect among gold miners in South Africa: a prevalence study with follow up of employment status. BMC. Public. Health. *15*, 1258. https://doi.org/10.1186/s12889-015-2566-8.

Langer, V., Vivi, E., Regensburger, D., Winkler, T.H., Waldner, M.J., Rath, T., Schmid, B., Skottke, L., Lee, S., Jeon, N.L., et al. (2019). IFN-gamma drives inflammatory bowel disease pathogenesis through VE-cadherin-directed vascular barrier disruption. J. Clin. Invest. *129*, 4691–4707. https://doi.org/10.1172/JCI124884.

Lee, S., Hayashi, H., Mastuzaki, H., Kumagai-Takei, N., and Otsuki, T. (2017). Silicosis and autoimmunity. Curr. Opin. Allergy. Clin. Immunol. *17*, 78–84. https://doi.org/10.1097/ACI.0000000000000350.

Leung, C.C., Yu, I.T.S., and Chen, W. (2012). Silicosis. Lancet *379*, 2008–2018. https://doi.org/10.1016/S0140-6736(12)60235-9.

Li, C., Du, S., Lu, Y., Lu, X., Liu, F., Chen, Y., Weng, D., and Chen, J. (2016). Blocking the 4-1BB pathway ameliorates crystalline silica-induced lung inflammation and fibrosis in mice. Theranostics *6*, 2052–2067. https://doi.org/10.7150/thno.16180.

Liu, S., Hao, C., Bao, L., Zhao, D., Zhang, H., Hou, J., Wang, D., Chen, H., Feng, F., and Yao, W. (2019). Silica particles mediate phenotypic and functional alteration of dendritic cells and induce

Th2 cell polarization. Front. Immunol. *10*, 787. https://doi.org/10.3389/fimmu.2019.00787.

Liu, X., Fang, S., Liu, H., Wang, X., Dai, X., Yin, Q., Yun, T., Wang, W., Zhang, Y., Liao, H., et al. (2015). Role of human pulmonary fibroblast-derived MCP-1 in cell activation and migration in experimental silicosis. Toxicol. Appl. Pharmacol. *288*, 152–160. https://doi.org/10.1016/j.taap.2015.07.002.

Luna-Gomes, T., Santana, P.T., and Coutinho-Silva, R. (2015). Silica-induced inflammasome activation in macrophages: role of ATP and P2X7 receptor. Immunobiology *220*, 1101–1106. https://doi.org/10.1016/j.imbio.2015.05.004.

Man, S.M., Karki, R., Sasai, M., Place, D.E., Kesavardhana, S., Temirov, J., Frase, S., Zhu, Q., Malireddi, R.S., Kuriakose, T., et al. (2016). IRGB10 liberates bacterial ligands for sensing by the AIM2 and caspase-11-NLRP3 inflammasomes. Cell *167*, 382–396.e17. https://doi.org/10.1016/j.cell.2016.09.012.

Meunier, E., Dick, M.S., Dreier, R.F., Schürmann, N., Broz, D.K., Warming, S., Roose-Girma, M., Bumann, D., Kayagaki, N., Takeda, K., et al. (2014). Caspase-11 activation requires lysis of pathogen-containing vacuoles by IFN-induced GTPases. Nature *509*, 366–370. https://doi.org/10.1038/nature13157.

Muñoz-Planillo, R., Kuffa, P., Martínez-Colón, G., Smith, B.L., Rajendiran, T.M., and Nunez, G. (2013). K(+) efflux is the common trigger of NLRP3 inflammasome activation by bacterial toxins and particulate matter. Immunity *38*, 1142–1153. https://doi.org/10.1016/j.immuni.2013.05.016.

Muszyńska - Graca, M., Dąbkowska, B., and Brewczyński, P. (2016). [Guidelines for the use of the international classification of radiographs of pneumoconioses of the international labour office (ILO): substantial changes in the currrent edition]. Med. Pregl. *67*, 833–837. https://doi.org/10.13075/mp.5893.00493.

Ohtsuka, Y., Wang, X.T., Saito, J., Ishida, T., and Munakata, M. (2006). Genetic linkage analysis of pulmonary fibrotic response to silica in mice. Eur. Respir. J. *28*, 1013–1019. https://doi.org/10.1183/09031936.06.00132505.

Pietras, E.M., Miller, L.S., Johnson, C.T., O'Connell, R.M., Dempsey, P.W., and Cheng, G. (2011). A MyD88-dependent IFNγR-CCR2 signaling circuit is required for mobilization of monocytes and host defense against systemic bacterial challenge. Cell. Res. *21*, 1068–1079. https://doi.org/10.1038/cr.2011.59.

Pollard, K.M. (2016). Silica, silicosis, and autoimmunity. Front. Immunol. *7*, 97. https://doi.org/10.3389/fimmu.2016.00097.

Salum, K.C.R., Castro, M.C.S., Moreira, V.B., Nani, A.S.F., and Kohlrausch, F.B. (2020a). Interleukin 1α and 1β gene variations are associated with tuberculosis in silica exposed subjects. Am. J. Ind. Med. *63*, 74–84. https://doi.org/10.1002/ajim.23066.

Salum, K.C.R., Castro, M.C.S., Nani, Â.S.F., and Kohlrausch, F.B. (2020b). Is individual genetic susceptibility a link between silica exposure and development or severity of silicosis? A systematic review. Inhal. Toxicol. *32*, 375–387. https://doi.org/10.1080/08958378.2020.1825569.

Schnettger, L., Rodgers, A., Repnik, U., Lai, R.P., Pei, G., Verdoes, M., Wilkinson, R.J., Young, D.B., and Gutierrez, M.G. (2017). A rab20-dependent membrane trafficking pathway controls M. tuberculosis replication by regulating phagosome spaciousness and integrity. Cell Host Microbe *21*, 619–628.e5. https://doi.org/10.1016/j.chom.2017.04.004.

Shenoy, A.R., Wellington, D.A., Kumar, P., Kassa, H., Booth, C.J., Cresswell, P., and MacMicking, J.D. (2012). GBP5 promotes NLRP3 inflammasome assembly and immunity in mammals. Science *336*, 481–485. https://doi.org/10.1126/science.1217141.

Slavov, E., Miteva, L., Prakova, G., Gidikova, P., and Stanilova, S. (2010). Correlation between TNF-alpha and IL-12p40-containing cytokines in silicosis. Toxicol. Ind. Health. *26*, 479–486. https://doi.org/10.1177/0748233710373082.

Su, X., Yu, Y., Zhong, Y., Giannopoulou, E.G., Hu, X., Liu, H., Cross, J.R., Rätsch, G., Rice, C.M., and Ivashkiv, L.B. (2015). Interferon-γ regulates cellular metabolism and mRNA translation to potentiate macrophage activation. Nat. Immunol. *16*, 838–849. https://doi.org/10.1038/ni.3205.

The LRM (2019). The world is failing on silicosis. Lancet Respir. Med. *7*, 283. https://doi.org/10.1016/S2213-2600(19)30078-5.

Wandel, M.P., Kim, B.H., Park, E.S., Boyle, K.B., Nayak, K., Lagrange, B., Herod, A., Henry, T., Zilbauer, M., Rohde, J., et al. (2020). Guanylate-binding proteins convert cytosolic bacteria into caspase-4 signaling platforms. Nat. Immunol. *21*, 880–891. https://doi.org/10.1038/s41590-020-0697-2.

Wang, D., Zhou, M., Liu, Y., Ma, J., Yang, M., Shi, T., and Chen, W. (2020). Comparison of risk of silicosis in metal mines and pottery factories. Chest *158*, 1050–1059. https://doi.org/10.1016/j.chest.2020.03.054.

Wang, Y.W., Lan, J.Y., Yang, L.Y., Wang De, J., and Kuang, J. (2012). TNF-alpha and IL-1RA polymorphisms and silicosis susceptibility in Chinese workers exposed to silica particles: a case-control study. Biomed. Environ. Sci. *25*, 517–525. https://doi.org/10.3967/0895-3988.2012.05.004.

Wu, F., Qu, Y., Tang, Y., Cao, D., Sun, P., Xia, Z., Department, O.O.H.A., Fudan, U., Ma'Anshan, I.A.S.C., School, O.P.H., et al. (2008). Lack of association between cytokine gene polymorphisms and silicosis and pulmonary tuberculosis in Chinese iron miners. J. Occup. Health *50*, 445–454. https://doi.org/10.1539/joh.L8006.

Wu, L., Luo, P.P., Tian, Y.H., Chen, L.Y., and Zhang, Y.L. (2022). Clinical efficacy of thymosin alpha 1 combined with multi-modality chemotherapy and its effects on immune function of patients with pulmonary tuberculosis complicated with diabetes. Pak. J. Med. Sci. *38*, 179–184. https://doi.org/10.12669/pjms.38.1.4419.

STAR★METHODS

KEY RESOURCES TABLE

REAGENT or RESOURCE	SOURCE	IDENTIFIER
Antibodies		
Anti-NLRP3 antibody	AdipoGen	Cat#: Cryo-2; RRID:AB_2490202
Anti-Caspase-1 antibody	Abcam	Cat#: ab179515; RRID:AB_2884954
Anti-IL1β antibody	R&D Systems	Cat#: AF-401-NA; RRID: AB_416684
Anti-LAMP1 antibody (clone 1D4B)	eBioscience	Cat#:14-1071-85; RRID: AB_65753
Anti-Rab7 antibody	Cell Signaling Technologies	Cat#: 9367S; RRID: AB_1904103
Anti-Cathepsin D antibody	Abcam	Cat# ab75852; RRID:AB_1523267
β-actin antibody (clone 8H10D10)	Cell Signaling Technologies	Cat#: 3700S; RRID: AB_2242334
Biological samples		
Human bronchoalveolar lavage fluid from exposure miners and silicosis patients	Hunan Prevention and Treatment Institute for Occupational Diseases	N/A
Chemicals, peptides, and recombinant proteins		
Ultra-pure LPS (*E. coli* 0111:B4)	InvivoGen	tlrl-3pelps
mouse recombinant interferon γ	R&D Systems	485-MI-100
mouse recombinant interferon α	R&D Systems	10149-IF-010
mouse recombinant interferon β	R&D Systems	8234-MB-010
Nano-SiO_2	InvivoGen	tlrl-sio
Fine ground silica	U.S. Silica	MIN-U-SIL 5
Aluminum crystal	InvivoGen	tlrl-aloh
Nigericin	InvivoGen	tlrl-nig
ATP	InvivoGen	tlrl-atpl
Poly (dA:dT)	InvivoGen	tlrl-patn
Flagellin	InvivoGen	tlrl-stfla
Leu-Leu-OMe·HCl	Chem-Impex International	Cat#: 04,578
Lipofectamine 3000 transfection reagent	Thermo Fisher Scientific	Cat#: L3000015
Alex594-labelled silica crystals	School of Chemistry, Nankai University	N/A
Critical commercial assays		
Multi-Analyte Flow Assay Kit	BioLegend	Cat#: 740150
Mouse IL-1α Uncoated ELISA Kit	InvivoGen	Cat#: 88-5019-88
Mouse IL-1β Uncoated ELISA Kit	InvivoGen	Cat#: 88-7013-88
Deposited data		
Human bronchoalveolar lavage fluid scRNA-Seq digital gene expression (DGE) matrix	This study	GEO: GSE174725
Experimental models: Cell lines		
Mouse macrophages	Prepared in B.L. Lab	Described in current manuscript
Experimental models: Organisms/strains		
C57BL/6 mice	Jackson Laboratory	Described in current manuscript
IFN-γ$R^{-/-}$ mice	Jackson Laboratory	Stock No: 003,288
IFN-αβ$R^{-/-}$ mice	Naval Medical University, China	Described in current manuscript
$NLRP3^{-/-}$ mice	Jackson Laboratory	Described in current manuscript
$IL\text{-}1R^{-/-}$ mice	Jackson Laboratory	Stock No: 003,245
IFN-γ$R^{-/-}$ $NLRP3^{-/-}$ mice	Described in current manuscript	Described in current manuscript

(*Continued on next page*)

Continued

REAGENT or RESOURCE	SOURCE	IDENTIFIER
IFN-γR$^{-/-}$ IL-1R$^{-/-}$ mice	Described in current manuscript	Described in current manuscript
Lyz2-cre^{+} mice	GemPharmatech	Described in current manuscript
IFN-γR$^{f/f}$ mice	Jackson Laboratory	Described in current manuscript
IFN-γR$^{f/f}$ *Lyz2-cre*$^{+}$ mice	Described in current manuscript	Described in current manuscript
Software and algorithms		
Cell Ranger v.4.0 (Human reference genome GRCh38)	10X Genomics	https://support.10xgenomics.com/single-cell-gene-expression
Seurat (R package) v.3.2	SatijaLab	https://satijalab.org/seurat
RadiAnt DICOM Viewer	Medixant	https://www.radiantviewer.com
ImageJ	NIH	https://imagej.nih.gov/ij/index.html
GraphPad Prism v.5	GraphPad Software	https://www.graphpad.com/scientific-software/prism/
FlowJo v.10	FlowJo	https://www.flowjo.com/solutions/flowjo/
LEGENDplex Data Analysis Software	BioLegend	https://www.biolegend.com/legendplex/

RESOURCE AVAILABILITY

Lead contact

Further information and requests for resources and reagents should be directed to and will be fulfilled by the lead contact, Fang Liang (liangfang924@163.com).

Materials availability

This study did not generate new unique reagents.

Data and code availability

The raw data, gene expression matrices, genotyping information and cell annotations have been deposited in the Gene Expression Omnibus (https://www.ncbi.nlm.nih.gov/geo/) under accession number GSE174725.

EXPERIMENTAL MODEL AND SUBJECT DETAILS

Clinical human samples

Patients were diagnosed with or without silicosis according to an occupational history of exposure to silica crystal, associated with radiologic studies with characteristic findings (standard chest X-ray with a profusion≥1/1 according to the ILO classification) and exclusion of other possible entities(Fernandez et al., 2015; Muszynska-Graca et al., 2016). A total of 42 patients including exposure co-workers (n = 19) and silicosis patients (n = 23) from Hunan Prevention and Treatment Institute for Occupational Diseases from August 2019 to December 2020 met the above conditions (Tables S1 and S2). The CT image were performed to differentiate the exposure mines and silicosis patients. The silicosis grades were defined as follows: exposure workers, no nodules present; grade I of silicosis patients, a few of nodules; grade II of silicosis patients, several nodules with calcified spots; grade III of silicosis patients, several nodules with calcified plaques. In addition, the miners that were diagnosed with silicosis will be undergo bronchoscopy examination and who are suffered to tuberculosis and lung cancer will be excluded. The bronchoalveolar lavage fluid was obtained immediately after lung washing therapy. This study was approved by the research ethics committee of the Third Xiangya Hospital of Central South University.

Mouse studies

Experimental protocols were approved by the Institutional Animal Care and Use Committees of the Central South University. WT mice, IFN-γR$^{-/-}$ mice, IFN-abR$^{-/-}$ mice, NLRP3$^{-/-}$ mice and IL-1R$^{-/-}$ mice on a C57BL/6J background were purchased from Jackson Laboratory. The IFN-γR/IL-1R$^{-/-}$ mice and IFN-γR/NLRP3$^{-/-}$ mice were obtained by interbred with the IFN-γR$^{-/-}$ mice and IL-1R$^{-/-}$ mice or the IFN-γR$^{-/-}$ mice and NLRP3$^{-/-}$ mice.

IFN-γR$^{fl/fl}$ mice (*IFN-γR*$^{fl/fl}$ allele) were purchased from Jax. *IFN-γR*$^{fl/fl}$ mice were interbred with heterozygous stud males (*Lys2-cre*$^{+}$, GemPharmatech Co. Ltd) to generate *IFN-γR*$^{fl/fl}$ *Lys2*-cre mice.

To obtained desired genotype, the targeted genome of F0 mice was amplified with PCR and sequenced and the offspring were crossed with wild-type C57BL/6 mice (GemPharmatech Co. Ltd) to obtain the heterozygous mice. The F1 heterozygous mice were further crossed with F1 heterozygous mice to generate F2 knockout mice and littermate WT mice. Transgenic mice used for experiments were confirmed to be desired genotype via standard genotyping techniques of tail DNA. The primer sequence is presented in Table S4. The male mice were used in our animal experiments.

Animals were maintained in a specific pathogen-free environment at the Department of Laboratory Animals of Central South University. In the current study, we used WT littermates as the controls for the transgenic mice. All experimental animal protocols were approved by the Institutional Animal Care and Use Committees of Central South University.

Macrophage preparation and stimulation

To obtain mouse peritoneal macrophages, mice (8-week-old) were injected with 3mL of sterile 3% thioglycollate broth intraperitoneally to elicit peritoneal macrophages. Cells were collected by lavage of the peritoneal cavity with 10 mL of RPMI medium 1640 (GIBCO) 72 h later. After washing, cells were resuspended in RPMI medium 1640 supplemented with 10% fetal bovine serum and antibiotics (GIBCO).

METHOD DETAILS

Analysis of bronchoalveolar lavage fluid cells by single cell RNA-seq

Bronchoalveolar lavage fluid cells from exposure and silicosis patients were counted and loaded onto the 10x device (10x Genomics). Cells were processed the manufacturer's protocol and sequenced on Illumina NextSeq sequencer. Sample demultiplexing, barcode processing, alignment, filtering, UMI counting, and aggregation of sequencing runs were performed using the Cell Ranger analysis pipeline (V4.1). Downstream analyses were performed in R using the Seurat package. For each cell, the total number of genes detected and the proportion of UMIs contributed by mitochondrially encoded transcripts were calculated to evaluate the cell quality. Cells in which fewer than 200 genes were detected and in which mitochondrially encoded transcripts constituted more than 10% of the total library were excluded from further analysis. To assess the genetic difference between samples, *t*-SNE projection was generated using 33,602 cells (including 19,453 from exposure miners and 14,149 cells from silicosis patients, Table S3). Mean and dispersion values were calculated for each gene across these cells, and a subset of 1,667 highly variable genes was selected for principal components analysis (PCA). Following PCA, the cell types were identified by the markers on CellMarker (http://biocc.hrbmu.edu.cn/CellMarker/) and yielded 9 clusters, including T cells (CD3^{+}), CD4^{+} T cells (CD3^{+} and CD4^{+}), CD8^{+} T cells (CD3^{+} and CD8^{+}), monocytes (CD14^{+}), macrophages (CD68^{+}), epithelial cell (EpCAM^{+}), neutrophil (CD11b^{+}), B cells (B220^{+}) and hemopoietic stem cells (HSCs, CD34^{+}). For classification of monocyte-macrophage populations, differential expression analysis was performed between each cluster and all other cells using a Wilcoxon rank sum test. The 11,643 monocyte-macrophages were selected and the differential expression analysis was performed between all monocyte-macrophages from exposure and silicosis patients using KEGG pathway analysis.

Fluorescent labeled silica nanoparticles

To obtained fuorescent labeled silica nanoparticles, 100ug of silica nanoparticles were mixed with 5ul of ammonia solution (20%) and 5mL of absolute ethanol, ultrasonic for 10-20 minutes, adjust the pH to around 8, then add 2ul of APTES under vigorous stirring, stir for 24 hours at 35 °C. Centrifuge the reaction solution at high speed under 10000 r/min, wash with ethanol for 3 times. Precipitate and suspend with 5mL of deionized water, add 2ul of dye NHS, and stir overnight at 25°C. The reaction solution was centrifuged at 6000 r/min for 3 minutes, the supernatant was discarded, then 5ml acetone was added to suspend precipitate, centrifuged at 10000 r/min for 10 minutes. The precipitate was washed alternately with ethanol and water to obtain fluorescent labeled silica nanoparticles.

Silica crystals and liposome-coated silica crystals

The silica crystals with a diameter of less than 0.1 μm used in cell stimulation was purchased from InvivoGen, and the ultrafine silica powder MIN-U-SIL 5 used in mice was purchased from U.S. SILICA. To obtained nano

silica crystals with a diameter less than 10 nm that used in our experiment, the silica crystal suspension was ultrasound at 100Hz to scatter the silica crystal dusts and performed a dialysis by regenerated cellulose (RC) membrane (5000D, Coolaber). To obtained liposome-coated silica crystals, the silica crystals were coated with P3000 (Invitrogen) and then encapsulated by liposome lipofectamine3000 (Invitrogen).

Silicosis model

To established silicosis mice model, male mice that were 25 to 30 g in weight were anaesthetized by 1% pentobarbital (50 mg/kg mice) and then fixed with mouse fixator. An aerosol injector was used to single orotracheal atomizing injection of silica crystals (200 mg/kg) suspension from the throat into the bronchus. Mice were exposed to silica crystals for 4 weeks to induce the development of silicosis. Mice in the control group were exposure to saline. At the end of time point, mice were anesthetized and performed micro-CT scanning or lung function test. The lung tissues were collected for pathological examination.

Macrophage stimulation

Peritoneal macrophages (10^6 cells per well) plated in 12-well plates were prestimulated with IFN-γ (25Unit/mL) for 16 hours before priming with ultra-pure LPS (1 ng/mL) for 4 h, and then stimulated with SiO_2 crystal (20 μg/mL) or Aluminum crystal (200ug/mL) for 6h, or pulsed with ATP (5 mM) or nigericin (10 μM) for 1 hour, or infected with live *E. coli* (MOI = 10) for 16 h (stop the bacteria growth by adding antibiotics into culture medium 2 h after infection). To study AIM2 inflammasome activation, IFN-γ-prestimulated macrophages were transfected with Poly (dA:dT) using Lipofectamine 3000 at a concentration of 1μM DNA plus 2.5μl Lipofectamine 3000 per ml. To study NLRC4 inflammasome activation, IFN-γ-prestimulated macrophages were transfected with flagellin (FLA) using Lipofectamine 3000 at a concentration of 2μM FLA plus 2.5μl Lipofectamine 3000 per ml. To study the role of type I interferon, macrophages were prestimulated with IFNα (25Unit/mL) or IFNβ (25Unit/mL) for 16 hours before priming with ultra-pure LPS (1 ng/mL) for 4 h, and then stimulated with SiO_2 crystal (20 μg/mL). To induce lysosomal disruption, Peritoneal macrophages were prestimulated with IFN-γ (25Unit/mL) for 16 hours before priming with ultra-pure LPS (1 ng/mL) for 4 hours, and then stimulated with Leu-Leu-OMe·HCl (1000μM, Chem-Impex International) for 5 hours. The peritoneal macrophages were stimulated with liposome-coated silica crystals for 4 hours to induce lysosomal disruption, for 6 hours to detect the IL-1β levels.

Micro-CT imaging

Before the scan, mice were anaesthetized by sodium pentobarbital (50 mg/kg) with sodium pentobarbital (50 mg/kg). Until complete relaxation, all animals were scanned with a micro-CT imaging technique. The micro-CT x-ray source was set to 50 kVp and 500 μA current. One hundred projections were acquired during 650 ms iso-pressure peak inspiration breath holds, with an exposure time of 450 ms per projection. All micro-CT images were visually inspected by a radiologist, who marked the location of all the nodules using the PointPicker2 ImageJ plugin.

Lung function

Before the test, mice were anaesthetized by sodium pentobarbital (50 mg/kg) with sodium pentobarbital (50 mg/kg). Until complete relaxation, all animals were performed with a standard catheter (CNS5002) provided by the Buxco equipment. After intubation or tracheostomy, mice were placed in a body plethysmograph and connected to a computer-controlled ventilator. The Buxco pulmonary function testing system (Buxco, Sharon, Connecticut, CT, USA) was used to analyze dynamic compliance (Cdyn), tidal volume (TV), minute volume (MV) and respiratory resistance index (RI) of the mice.

H&E and masson staining

The lung tissues were fixed in 4% neutral formalin solution for 48 h. The samples were sequentially dehydrated, embedded in paraffin, and cut into 4 μm sections. The pathologic and morphologic characteristics of the tissues were observed by haematoxylin & eosin (H&E) and Masson staining. The areas fraction of granuloma that was detected by H&E staining were determined by the cell-counting across random non co-incident microscopic fields at a magnification of ×200. Polymorphonuclear, mononuclear and total cells in lung parenchyma and granuloma were evaluated at x1,000 magnification. The thresholds for collagen fibres that were detected by Masson staining were established after the contrast was enhanced up to a point at which the fibres were easily identified as birefringent bands. The area occupied by collagen fibres was determined by digital densitometric recognition. Bronchi and blood vessels were carefully avoided

during the measurements. The area occupied by fibres was divided by tissue area and expressed as fraction area of collagen fibres. Four same visual fields of H&E and Masson staining in one mouse were selected to evaluated the level of lung fibrosis.

Cytometric Bead Array

Mice were exposed to 50 μl suspensions of 5000 μg of silica crystals in PBS by direct orotracheal instillation. Control mice received PBS. Animals were sacrificed 3 days after instillation and a bronchoalveolar lavage (BAL) was carried out by repeatedly instillating and withdrawing 1 ml of 1% BSA/PBS solution three consecutive times. Cytokine levels of BAL were measured using a Multiplex Luminex assay (BD sciences). Reagents for quantitative ProcartaPlex Luminex immunoassay were sourced from Affymetrix eBioscience. Cytometric Bead Array (Bio-legend) were used according to the manufacturer's instructions. and results were read on the Bio-Plex 200 instrument. In order to set up the heatmap, the heatmap value of same cytokines was calculated as a fraction of the highest detected cytokines levels relative to the detected cytokines levels.

ELISA

Cell culture supernatant samples were analyzed using IL-1α and IL-1β ELISA kits (Invitrogen).

Immunoblotting

Proteins from cell-free supernatants were extracted by methanol-chloroform precipitation and cell extracts. Samples were separated by SDS-PAGE and transferred onto PVDF membranes (Millipore). Antibodies to mouse caspase-1 (Abcam) were used at 1:1000 dilution, IL-1β (RD systems) was used at 1:1000 dilution. Antibodies to mouse NLRP3 (adipogen) was used at 1:1000. Antibodies to LAMP1 (eBioscience), Rab7 (CST) and cathepsin D (Abcam) were used at 1:1000 dilution. Blots were normalized to β-actin expression.

Flow cytometry

For evaluation of lysosomal rupture, macrophage cells were incubated with 1 μg/mL acridine orange for15 min, washed three times and subsequently stimulated as indicated. Lysosomal rupture can be assessed by loss of emission at 600–650 nm using flow cytometry. All flow cytometry experiments were performed on an LSRII cytometer (BD Biosciences). Data were acquired by DIVA (BD Biosciences) and analyzed by FlowJo software (Tree Star Inc., Ashland, OR).

Quantification of silica crystals/phagosomal area

For the stereological analysis of the silica crystals/phagosomal area, each phagosomal area and the silica crystal area that included in same phagosomal region were separately circled and circulated by ImageJ software. Each relative volume silica crystal in independent phagosomes was calculated as a fraction of silica crystal area relative to the phagosomal area. A minimum of 30 profiles of different silica crystals/phagosomal area was analyzed per sample.

QUANTIFICATION AND STATISTICAL ANALYSIS

All data were analyzed using GraphPad Prism software (version 5.01). Data were analyzed using by Student's t test were used for comparison between two groups or one-way ANOVA followed by post hoc Bonferroni test for multiple comparisons. p value <0.05 was considered statistically significant for all experiments. All values are presented as the mean $\pm$ SD